





Gapped Dirac materials and quantum valley currents in dual-gated hBN/bilayer-graphene heterostructures

Takuya Iwasaki ^{1,*}, Yoshifumi Morita ², Kenji Watanabe ³, and Takashi Taniguchi ¹

¹Research Center for Materials Nanoarchitectonics, National Institute for Materials Science (NIMS),
1-1 Namiki, Tsukuba, Ibaraki 305-0044, Japan

²Faculty of Engineering, Gunma University, Kiryu, Gunma 376-8515, Japan

³Research Center for Electronic and Optical Materials, NIMS, 1-1 Namiki, Tsukuba, Ibaraki 305-0044, Japan



(Received 25 October 2023; revised 6 January 2024; accepted 9 January 2024; published 8 February 2024)

In gapped Dirac materials, the topological current associated with each valley can flow in opposite directions creating long-range charge-neutral valley currents. We report valley currents in hexagonal boron nitride (hBN)/bilayer-graphene heterostructures with an energy gap, which is tunable by a perpendicular electric (displacement) field in a dual-gated structure. We observed significant nonlocal resistance, consistent with the scaling theory of the valley Hall effect. In the low-temperature limit, the nonlocal resistance approaches a saturated value near the “quantum limit,” indicating the emergence of quantum valley currents.

DOI: [10.1103/PhysRevB.109.075409](https://doi.org/10.1103/PhysRevB.109.075409)

I. INTRODUCTION

A valley (degenerate local minimum/maximum in the conduction/valence band, respectively) is a quantum-mechanical degree of freedom built into electrons for several solid-state systems, which is referred to as K and K' in the case of graphene [1]. In the context of graphene, the valley degree of freedom is sometimes referred to as “flavor” combined with the spin degree of freedom.

Graphene, a monolayer of carbon atoms, is the parent of low-dimensional quantum metamaterial [2]. Single-layer graphene (SLG) has relativistic energy bands with a linear dispersion in the low-energy limit, whereas its bilayer counterpart, AB -stacked (Bernal) bilayer graphene (BLG), has degenerate energy bands with a parabolic energy touching. Both SLG and BLG [and their heterostructures with hexagonal boron nitride (hBN) [3,4]] belong to a “Dirac-material family,” although the detailed character of each material varies even within the family. Gapped Dirac materials can exhibit topological current transverse to the applied electric field even without a magnetic field or broken time-reversal symmetry. In the case of graphene, the topological current associated with each valley of an energy band can flow in opposite directions. This phenomenon is known as the valley Hall effect (VHE), which generates long-range charge-neutral valley currents. The electrical VHE was demonstrated for hBN/SLG superlattices [5,6]. The VHE has also been observed in BLG under a perpendicular electric field [7,8]. In contrast to SLG, BLG provides an ideal platform for detailed study of valley currents because the energy gap and band structure can be systematically tuned by a perpendicular electric field [9]. The topological valley current was also observed in hBN/BLG superlattices [10]. A more recent study reported the observation

of valley currents with a systematic control of the crystallographic stacking angle between hBN and BLG [11].

Here, we focus on dual-gated hBN/BLG heterostructures in which the energy gap is further tuned by applying a perpendicular displacement field. We demonstrate the detection and manipulation of the valley current with a tunable displacement field. The scaling analysis indicates that the VHE is established in the temperature range below the band gap. In the low-temperature limit, the nonlocal resistance approaches the “quantum limit,” implying the emergence of quantum valley currents [6].

II. METHODS

To fabricate the devices, BLG and hBN flakes were first prepared on a SiO_2 /heavily doped Si substrate by mechanical exfoliation from bulk crystals. The hBN/BLG/hBN heterostructure was assembled by a dry transfer method [12]. The top gate (Ti/Au) was fabricated via electron beam (EB) lithography and EB deposition. The heterostructure was then patterned into a Hall bar geometry using EB lithography and reactive ion etching (CHF_3/O_2 plasma). The edge contact electrodes (Cr/Au) were likewise fabricated via EB lithography and EB deposition [13].

To investigate the transport properties, we adopted a four-terminal configuration with AC lock-in techniques. The device was measured in a ^4He cryostat with a variable temperature insert to control the temperature (T). A superconducting magnet was used to apply a magnetic field (B) perpendicularly to the BLG plane.

The schematic cross section of our device is shown in Fig. 1(a). Our devices comprise the hBN/BLG/hBN heterostructure with the top and the bottom gates (so-called “dual-gated structure”), where the hBN layers play the role of a high-quality dielectric on both sides. The thicknesses of the top and bottom hBN layers are 35 and 34 nm, respectively,

*IWASAKI.Takuya@nims.go.jp

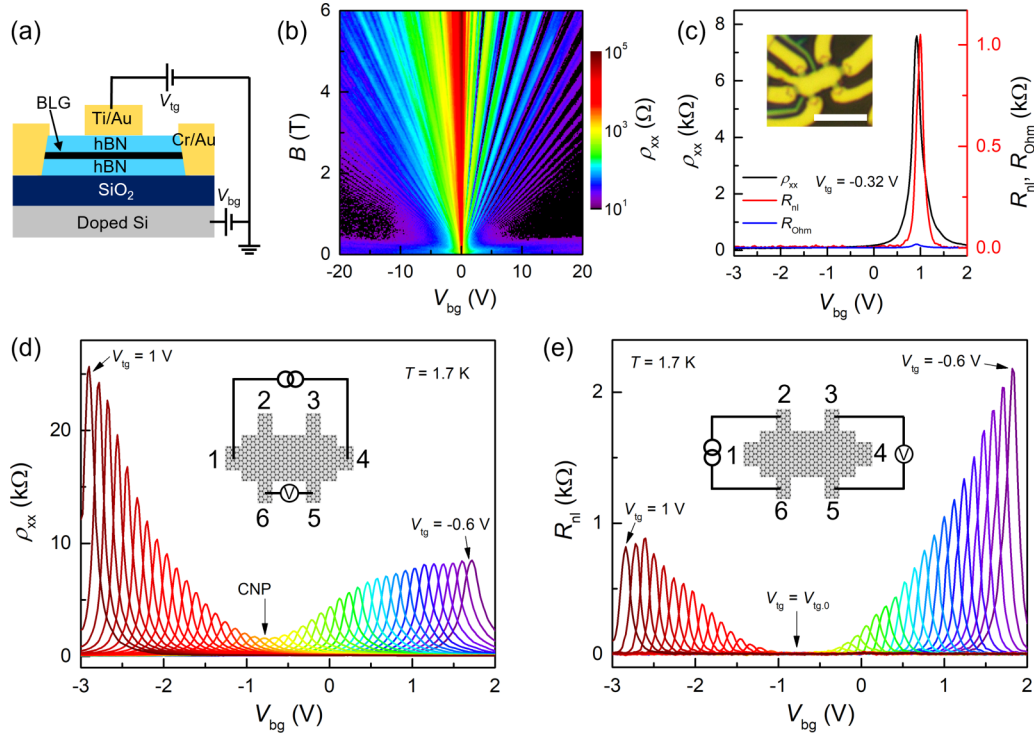


FIG. 1. (a) Schematic cross section of the device. (b) Landau fan diagram: the intensity map of ρ_{xx} as a function of V_{bg} and B at $T = 1.7$ K and $V_{tg} = 0$ V. (c) ρ_{xx} (black), R_{nl} (red), and R_{Ohm} (blue) as a function of V_{bg} at $T = 1.7$ K, $B = 0$ T, and $V_{tg} = -0.32$ V. The inset shows the optical image of the device. The scale bar corresponds to $5 \mu\text{m}$. (d) ρ_{xx} as a function of V_{bg} for V_{tg} from -0.6 to 1 V. The inset shows the schematic of the local measurement configuration. (e) Same plot as (d) for the nonlocal configuration.

which is confirmed by an atomic force microscope. Highly doped Si was used as a back gate. By applying top-gate (V_{tg}) and back-gate voltage (V_{bg}) to the BLG, the perpendicular displacement field (D) and carrier density (n) are independently controlled, where $D = [C_{bg}(V_{bg} - V_{bg,0}) - C_{tg}(V_{tg} - V_{tg,0})]/2\epsilon_0$, and $n = [C_{bg}(V_{bg} - V_{bg,0}) + C_{tg}(V_{tg} - V_{tg,0})]/e$; $C_{bg(tg)}$ is the back/top gate capacitance per unit area, $V_{bg,0(tg,0)}$ is the offset from the charge neutrality point (CNP), ϵ_0 is the vacuum permittivity, and e is the elementary charge.

We fabricated two Hall bar devices D1 and D2, both of which yield fundamentally consistent results. In the main text, we focus on the characteristics of D1 (see Supplemental Material S2 for D2 [14]). The optical image of D1 is displayed in the inset of Fig. 1(c). The channel length and width of D1 are $L = 2.5 \mu\text{m}$ and $W = 1.6 \mu\text{m}$, respectively.

III. RESULTS AND DISCUSSION

Figure 1(b) shows the intensity map of the longitudinal resistivity ρ_{xx} as a function of V_{bg} and B at $T = 1.7$ K, where $\rho_{xx} = V_{65}/I_{14} \times (W/L)$ [see also the inset in Fig. 1(d)], V_{kl} is the voltage drop between terminals k and l , and I_{ij} is the current injected between terminals i and j . The peak with a high ρ_{xx} at $V_{bg} \sim -0.78$ V corresponds to the CNP. We observe a typical Landau quantization spectrum of BLG fanning out from the CNP [21]. The carrier mobility estimated from Hall measurements at $T = 1.7$ K is $\sim 23 \text{ m}^2 \text{ V}^{-1} \text{ s}^{-1}$ for electrons and $\sim 19 \text{ m}^2 \text{ V}^{-1} \text{ s}^{-1}$ for holes. The residual carrier density is $\sim 3.6 \times 10^{10} \text{ cm}^{-2}$, which is estimated from the full width at half maximum of the CNP peak [22]. These data indicate

that our device is in an ultraclean regime (see Supplemental Material S1 for the high-quality properties of D1 in more detail, including the mean free path and the quantum Hall effect [14]).

The valley currents manifest themselves through nonlocal transport properties in the Hall-bar geometry [see the inset of Fig. 1(e)]. In BLG with an energy gap, near the valleys of the energy bands, a finite Berry curvature emerges with an opposite sign in each valley [1]. The Berry curvature, playing the role of a (pseudo)magnetic field in the momentum space, induces anomalous velocity with an opposite direction to electrons in each valley. Therefore, in nonlocal measurements, a transverse neutral valley current is generated by the electric current between the left-side terminals (VHE). This valley current is converted into a voltage drop between the right-side terminals (inverse VHE). As illustrated in Fig. 1(c), a finite nonlocal resistance $R_{nl} = V_{53}/I_{62}$ [see also the inset in Fig. 1(e) for the measurement configuration] is observed near the CNP of the local resistivity (ρ_{xx}). In general, nonlocal resistance can be attributed to the contribution from stray charge currents via the van der Pauw formula $R_{Ohm} = (\rho_{xx}/\pi) \exp(-\pi L/W)$. In our device, such a contribution is negligible, as shown in Fig. 1(c). The R_{nl} peak is sharper than that of ρ_{xx} and is consistent with previous studies on the VHE [5–8, 10]. Combined with the scaling analysis below, we attribute the nonlocal response observed in our device to the emergence of the valley current.

For the local measurement configuration, the increase of ρ_{xx} with an application of D is observed in Fig. 1(d), which corresponds to a gap opening at the CNP in BLG [9]. The

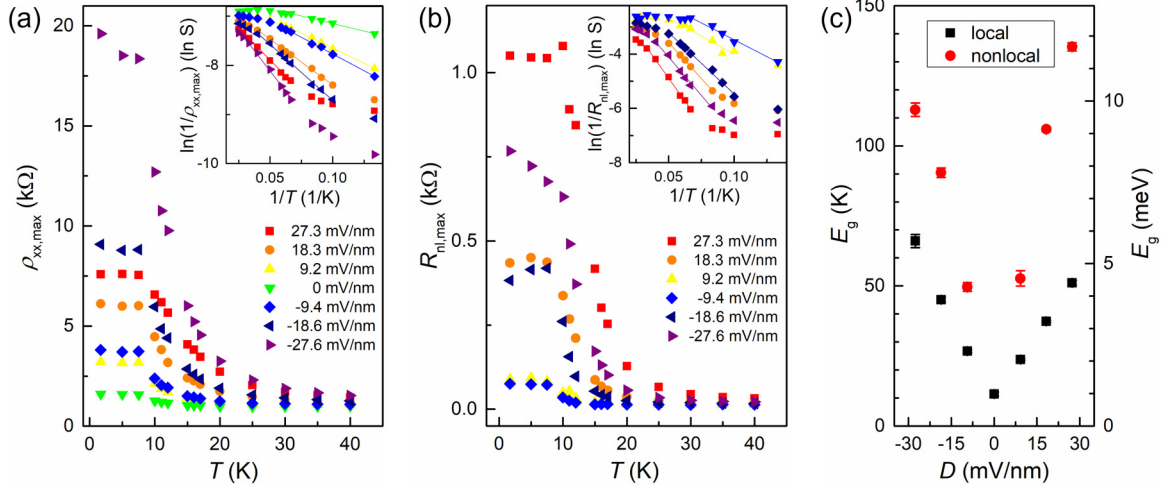


FIG. 2. (a),(b) Temperature dependence of (a) ρ_{xx} and (b) R_{nl} for various D . The insets show the Arrhenius plots for (a) $\rho_{xx,\max}$ and (b) $R_{nl,\max}$, respectively. The solid lines show the fitting to $\sim \exp(-E_g/2k_B T)$. (c) Energy gap extracted from the Arrhenius fit for $\rho_{xx,\max}$ (local, black) and $R_{nl,\max}$ (nonlocal, red) as a function of D . The error bars correspond to the ambiguity in the fitting procedure.

asymmetric increase in ρ_{xx} depending on the polarity (sign) of D can be attributed to different dielectric environments between the top and back gates in our device. For the nonlocal measurement configuration shown in Fig. 1(e), the R_{nl} peak appears for $|D| > 6$ mV/nm. The maximum R_{nl} increases with larger $|D|$ and reaches an order of k Ω at $D \sim 27$ mV/nm [see also Fig. 2(b) to confirm the numeric relationship of D vs. R_{nl}]. As shown in Refs. [7,8], without an alignment between hBN and BLG, the nonlocal resistance is strongly suppressed to a near-zero value in a small displacement-field regime. To be more precise, the nonlocal resistance cannot be distinguished from the small Ohmic contribution. In our device D1, the nonlocal resistance is enhanced even under such a small displacement field. In addition, in another device D2, the data show a finite nonlocal resistance even under zero displacement field (see Supplemental Material S2). The device D2 is close to D1 in the alignment angle since they are from the same stack. The increase of the R_{nl} with a different polarity in D is also asymmetric here, but exhibits an opposite behavior to that of ρ_{xx} . Detailed study of these trends is left as a future task. As commented on above, different dielectric environments between the top and back gates may play some role here. The sign of D should correspond to the difference in the shift of low-energy electronic states toward (or away from) the top and bottom hBN's with different settings (width, alignment, etc.). Compared with the nonlocal resistance of conventional BLG for the same D [7,8], the threshold of D for a finite R_{nl} is smaller, and the maximum value of R_{nl} is much higher in our device, approaching the “quantum limit” as discussed below. The R_{nl} reaches a k Ω order at maximum, indicating that the nonlocal resistance is approaching the quantum limit [6]. At the quantum limit, the nonlocal resistance illustrates an order of $\sim h/4e^2$ (h is the Planck constant) apart from a prefactor of order 1, which also implies a large valley Hall angle. In this study, as discussed in Ref. [6], we ascribe this to “quantum” valley currents.

Let us now discuss the T dependence. In Figs. 2(a) and 2(b), the T dependence of maximum ρ_{xx} ($\rho_{xx,\max}$) and R_{nl} ($R_{nl,\max}$) demonstrates a thermally activated behavior in the

high- T regime. The T dependence of $\rho_{xx,\max}$ and $R_{nl,\max}$ becomes weak in the low- T regime, where hopping conduction dominates. Moreover, the temperature at which the conduction mechanism switches between thermal activation and hopping conduction becomes higher for larger $|D|$. This T dependence is consistent with previous studies on BLG [7,8]. Using the Arrhenius fit, i.e., $1/\rho_{xx,\max}$ or $1/R_{nl,\max} \sim \exp(-E_g/2k_B T)$ (where E_g is the energy gap and k_B is the Boltzmann constant) for the high- T regime [insets in Figs. 2(a) and 2(b)], the energy gaps for local ($E_{g,\text{local}}$) and nonlocal configuration ($E_{g,\text{nl}}$) are extracted and summarized in Fig. 2(c). For both local and nonlocal configurations, E_g increases with the application of finite $|D|$. At $D = 0$, E_g is ~ 11 K and comparable with previous reports on different hBN/BLG superlattices with a small misalignment [10]. This is consistent with the observation of the “Umklapp effects” in resistivity (discussed in Supplemental Material S3 [14]). The finite energy gap and the Umklapp effects are absent with a large misalignment between hBN and BLG [23] (see Supplemental Material S4 for the alignment between hBN and BLG in our device [14]). At $D = 0$, E_g is well defined only for the local configuration, since $R_{nl,\max} \sim 0$ and the energy gap is difficult to define here [Fig. 1(e)]. When the local conductivity ($\sigma_{xx} = \rho_{xx}^{-1}$) exceeds the valley Hall conductivity (σ_{xy}^v), i.e., $\sigma_{xx} \gg \sigma_{xy}^v$, the nonlocal resistance is described by the following formula [24]:

$$R_{nl} = \frac{W}{2l_v} (\sigma_{xy}^v)^2 \rho_{xx}^3 \exp\left(-\frac{L}{l_v}\right), \quad (1)$$

where l_v is the intervalley scattering length. Thus, $E_{g,\text{nl}} \sim 3E_{g,\text{local}}$ is expected. In our data, $E_{g,\text{nl}}$ is approximately three times larger than $E_{g,\text{local}}$ for $D \geq 18.3$ mV/nm [e.g., $E_{g,\text{nl}} \sim (2.88 \pm 0.05)E_{g,\text{local}}$ at $D = 18.3$ mV/nm, $E_{g,\text{nl}} \sim (2.72 \pm 0.07)E_{g,\text{local}}$ at $D = 27.3$ mV/nm, the error is estimated by the Arrhenius fitting], which demonstrates a consistent trend.

Next, we discuss the scaling relation between $R_{nl,\max}$ and $\rho_{xx,\max}$. As expected from Eq. (1), the cubic scaling relation between $R_{nl,\max}$ and $\rho_{xx,\max}$ is found in the range $T = 12$ – 25 K

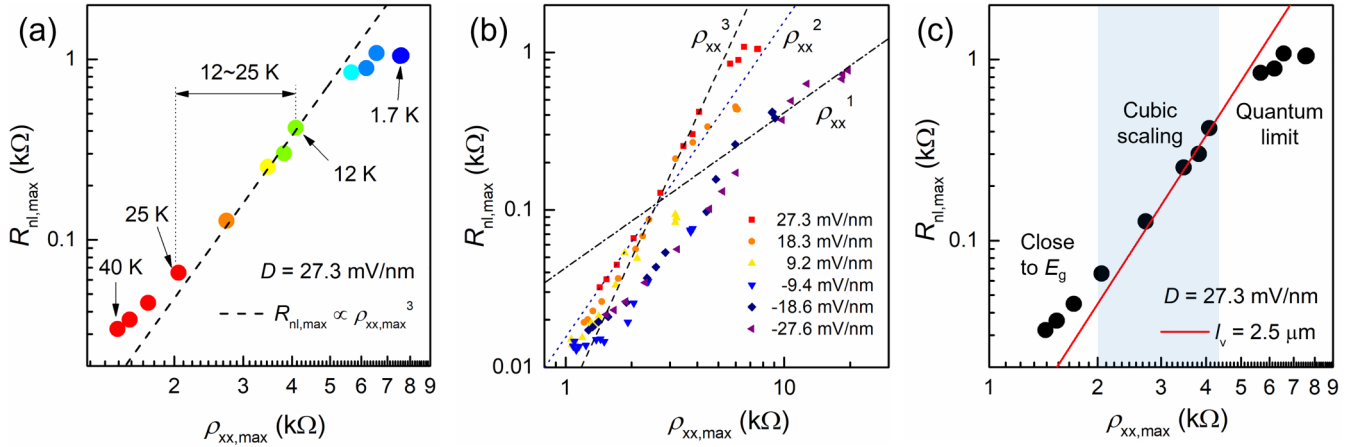


FIG. 3. Scaling analysis in the log-log plot between $\rho_{xx,max}$ and $R_{nl,max}$. The data are obtained from each T ranging 1.7–40 K. (a) At $D = 27.3$ mV/nm. The dashed line represents a fitting to the cubic relation ($\sim \rho_{xx,max}^3$). (b) The same as (a) with various D . The dashed, dotted, and dot-dashed lines correspond to the relation $\sim \rho_{xx,max}^3$, $\sim \rho_{xx,max}^2$, and $\sim \rho_{xx,max}^1$, respectively. (c) At $D = 27.3$ mV/nm. The solid line illustrates the fitting result with $p = 3.09$, $L = 2.5$ μm , $W = 1.6$ μm , and $l_v = 2.5$ μm .

at $D = 27.3$ mV/nm [Fig. 3(a)]. In the higher- T regime, the valley Hall conductivity should exhibit a deviation from the quantum value, and it is reasonable that the cubic scaling does not hold. In the low- T limit, the nonlocal resistance can approach a saturated value in the quantum limit. Moreover, our data for $D \geq 18.3$ mV/nm display the cubic scaling relation in the intermediate- T regime as illustrated in Fig. 3(b). This D range is the same as one for which $E_{g,nl} \sim 3E_{g,local}$ holds [Fig. 2(c)], as discussed above. In the T range below the $E_{g,local}$, it is reasonable to assume $\sigma_{xy}^v = 4e^2/h$ at the CNP [11]. Plugging this σ_{xy}^v into Eq. (1), the nonlocal resistance can be described by $R_{nl} = \rho_{xx}^p (W/2l_v)(4e^2/h)^2 \exp(-L/l_v)$, where p is ideally 3 and actually, we treat it as a fitting parameter. By fitting this formula to our data in the range where the cubic scaling relation holds, i.e., $p \sim 3$ [Fig. 3(c)], we obtain $l_v = 2.5$ μm , which is near the scale of our device and compatible with a previous report (e.g., [5]).

Comments are in order on some ambiguity in the weak- D regime; we note that, when the gap is small, disorder effects can obscure a clear scaling relation even in ultraclean devices and, moreover, a precursor toward possible phase transition/instability can play some role. In our recent work [25], we revealed that in the phase diagram of hBN/BLG superlattices the weak- D regime is a “bifurcation” point of phase boundaries, where some theories ascribe such instabilities to competing orders [26–29].

Finally, let us comment more on the “quantum limit” terminology [6]. For $\sigma_{xx} \ll \sigma_{xy}^v$ (the valley Hall angle $\sim \pi/2$), $R_{nl} = (W/2l_v)h/4e^2$ was proposed [30]. In real settings, empirically in ultraclean devices, W and l_v are of the same order, which is also reconfirmed in our setting. As discussed above, the cubic scaling was verified in the regime where the R_{nl} is small (small/moderate valley Hall angle). On the other hand, when the valley Hall angle is large, the nonlocal resistance can exhibit an order of $\sim h/4e^2$, i.e., approaching the quantum

limit near $R_{nl} \sim 2.1$ k Ω for this device. In Ref. [6], a possible scenario of the edge-mode conduction was proposed deeply inside the quantum limit. Since our outputs are still below the genuine quantum limit, we presume that bulk conduction still dominates the transport properties in this regime and the scaling relations hold. On the other hand, when the scaling relation breaks, a possible scenario is the edge-conduction picture [6].

IV. SUMMARY

We investigated the local and nonlocal transport properties in dual-gated hBN/BLG heterostructures, which belong to gapped Dirac materials. The observation of giant nonlocal resistance is consistent with the scaling theory of the valley Hall effect. In the low-temperature limit, on the other hand, we observed nonlocal resistance near the quantum limit. To elucidate the conduction mechanism (“edge vs bulk,” etc.) in this low-temperature limit, further experiments with multiterminal devices and theoretical modeling are crucial. Our work should lay a sound basis for next-generation devices based on quantum metamaterials with nanostructures like the quantum dot, point contact, and their hybrids.

ACKNOWLEDGMENTS

The authors thank H. Osato, E. Watanabe, and D. Tsuya from the NIMS Nanofabrication Facility for discussing the device fabrication. This work was partially supported by JPSJ KAKENHI Grant No. 21H01400, and “Advanced Research Infrastructure for Materials and Nanotechnology in Japan (ARIM)” of the Ministry of Education, Culture, Sports, Science and Technology (MEXT), Proposal No. JPMXP1223NM5186.

- [1] D. Xiao, W. Yao, and Q. Niu, Valley-Contrasting physics in graphene: Magnetic moment and topological transport, *Phys. Rev. Lett.* **99**, 236809 (2007).
- [2] A. K. Geim and K. S. Novoselov, The rise of graphene, *Nat. Mater.* **6**, 183 (2007).
- [3] K. Watanabe, T. Taniguchi, and H. Kanda, Direct-bandgap properties and evidence for ultraviolet lasing of hexagonal boron nitride single crystal, *Nat. Mater.* **3**, 404 (2004).
- [4] C. R. Dean, A. F. Young, I. Meric, C. Lee, L. Wang, S. Sorgenfrei, K. Watanabe, T. Taniguchi, P. Kim, K. L. Shepard, and J. Hone, Boron nitride substrates for high-quality graphene electronics, *Nat. Nanotechnol.* **5**, 722 (2010).
- [5] R. V. Gorbachev, J. C. W. Song, G. L. Yu, A. V. Kretinin, F. Withers, Y. Cao, A. Mishchenko, I. V. Grigorieva, K. S. Novoselov, L. S. Levitov, and A. K. Geim, Detecting topological currents in graphene superlattices, *Science* **346**, 448 (2014).
- [6] K. Komatsu, Y. Morita, E. Watanabe, D. Tsuya, K. Watanabe, T. Taniguchi, and S. Moriyama, Observation of the quantum valley Hall state in ballistic graphene superlattices, *Sci. Adv.* **4**, eaaq0194 (2018).
- [7] M. Sui, G. Chen, L. Ma, W.-Y. Shan, D. Tian, K. Watanabe, T. Taniguchi, X. Jin, W. Yao, D. Xiao, and Y. Zhang, Gate-tunable topological valley transport in bilayer graphene, *Nat. Phys.* **11**, 1027 (2015).
- [8] Y. Shimazaki, M. Yamamoto, I. V. Borzenets, K. Watanabe, T. Taniguchi, and S. Tarucha, Generation and detection of pure valley current by electrically induced Berry curvature in bilayer graphene, *Nat. Phys.* **11**, 1032 (2015).
- [9] Y. Zhang, T.-T. Tang, C. Girit, Z. Hao, M. C. Martin, A. Zettl, M. F. Crommie, Y. Ron Shen, and F. Wang, Direct observation of a widely tunable bandgap in bilayer graphene, *Nature (London)* **459**, 820 (2009).
- [10] K. Endo, K. Komatsu, T. Iwasaki, E. Watanabe, D. Tsuya, K. Watanabe, T. Taniguchi, Y. Noguchi, Y. Wakayama, Y. Morita, and S. Moriyama, Topological valley currents in bilayer graphene/hexagonal boron nitride superlattices, *Appl. Phys. Lett.* **114**, 243105 (2019).
- [11] E. Arrighi, V.-H. Nguyen, M. Di Luca, G. Maffione, Y. Hong, L. Farrar, K. Watanabe, T. Taniguchi, D. Maily, J.-C. Charlier, and R. Ribeiro-Palau, Non-identical moiré twins in bilayer graphene, *Nat. Commun.* **14**, 8178 (2023).
- [12] T. Iwasaki, K. Endo, E. Watanabe, D. Tsuya, Y. Morita, S. Nakaharai, Y. Noguchi, Y. Wakayama, K. Watanabe, T. Taniguchi, and S. Moriyama, Bubble-Free transfer technique for high-quality graphene/hexagonal boron nitride van der Waals heterostructures, *ACS Appl. Mater. Interfaces* **12**, 8533 (2020).
- [13] L. Wang, I. Meric, P. Y. Huang, Q. Gao, Y. Gao, H. Tran, T. Taniguchi, K. Watanabe, L. M. Campos, D. A. Muller, J. Guo, P. Kim, J. Hone, K. L. Shepard, and C. R. Dean, One-dimensional electrical contact to a two-dimensional material, *Science* **342**, 614 (2013).
- [14] See Supplemental Material at <http://link.aps.org/supplemental/10.1103/PhysRevB.109.075409> for the high-quality properties of device D1 in more detail, the characterization of device D2, the temperature dependence of the resistivity away from the CNP, and the alignment between hBN and BLG (see also Refs. [15–20] therein).
- [15] E. H. Hwang and S. Das Sarma, Acoustic phonon scattering limited carrier mobility in two-dimensional extrinsic graphene, *Phys. Rev. B* **77**, 115449 (2008).
- [16] S. Das Sarma, S. Adam, E. H. Hwang, and E. Rossi, Electronic transport in two-dimensional graphene, *Rev. Mod. Phys.* **83**, 407 (2011).
- [17] K. Kadowaki and S. B. Woods, Universal relationship of the resistivity and specific heat in heavy Fermion compounds, *Solid State Commun.* **58**, 507 (1986).
- [18] J. R. Wallbank, R. Krishna Kumar, M. Holwill, Z. Wang, G. H. Auton, J. Birkbeck, A. Mishchenko, L. A. Ponomarenko, K. Watanabe, T. Taniguchi, K. S. Novoselov, I. L. Aleiner, A. K. Geim, and V. I. Fal'ko, Excess resistivity in graphene superlattices caused by Umklapp electron-electron scattering, *Nat. Phys.* **15**, 32 (2019).
- [19] M. Kuri, S. K. Srivastav, S. Ray, K. Watanabe, T. Taniguchi, T. Das, and A. Das, Enhanced electron-phonon coupling in doubly aligned hexagonal boron nitride bilayer graphene heterostructure, *Phys. Rev. B* **103**, 115419 (2021).
- [20] D. Wang, G. Chen, C. Li, M. Cheng, W. Yang, S. Wu, G. Xie, J. Zhang, J. Zhao, X. Lu, P. Chen, G. Wang, J. Meng, J. Tang, R. Yang, C. He, D. Liu, D. Shi, K. Watanabe, T. Taniguchi, J. Feng, Y. Zhang, and G. Zhang, Thermally induced graphene rotation on hexagonal boron nitride, *Phys. Rev. Lett.* **116**, 126101 (2016).
- [21] K. S. Novoselov, E. McCann, S. V. Morozov, V. I. Fal'ko, M. I. Katsnelson, U. Zeitler, D. Jiang, F. Schedin, and A. K. Geim, Unconventional quantum Hall effect and Berry's phase of 2π in bilayer graphene, *Nat. Phys.* **2**, 177 (2006).
- [22] K. I. Bolotin, K. J. Sikes, Z. Jiang, M. Klima, G. Fudenberg, J. Hone, P. Kim, and H. L. Stormer, Ultrahigh electron mobility in suspended graphene, *Solid State Commun.* **146**, 351 (2008).
- [23] C. Moulds and V. Fal'ko, Umklapp electron-electron scattering in bilayer graphene moiré superlattice, *Phys. Rev. B* **107**, 144111 (2023).
- [24] D. A. Abanin, A. V. Shytov, L. S. Levitov, and B. I. Halperin, Nonlocal charge transport mediated by spin diffusion in the spin Hall effect regime, *Phys. Rev. B* **79**, 035304 (2009).
- [25] T. Iwasaki, Y. Morita, K. Watanabe, and T. Taniguchi, Dual-gated hBN/bilayer-graphene superlattices and the transitions between the insulating phases at the charge neutrality point, *Phys. Rev. B* **106**, 165134 (2022).
- [26] R. Nandkishore and L. Levitov, Flavor symmetry and competing orders in bilayer graphene, [arXiv:1002.1966](https://arxiv.org/abs/1002.1966).
- [27] R. Nandkishore and L. Levitov, Quantum anomalous Hall state in bilayer graphene, *Phys. Rev. B* **82**, 115124 (2010).
- [28] R. Nandkishore and L. Levitov, Dynamical screening and excitonic instability in bilayer graphene, *Phys. Rev. Lett.* **104**, 156803 (2010).
- [29] Z. Dong and L. Levitov, Chiral Stoner magnetism in Dirac bands, [arXiv:2208.02051](https://arxiv.org/abs/2208.02051).
- [30] M. Beconcini, F. Taddei, and M. Polini, Nonlocal topological valley transport at large valley Hall angles, *Phys. Rev. B* **94**, 121408(R) (2016).